Metrol. Meas. Syst., Vol. 31 (2024) No. 4, pp. 637–655
DOI: 10.24425/mms.2024.152045

PAN POLSKA AKADEMIA NAUK

METROLOGY AND MEASUREMENT SYSTEMS
Index 330930, ISSN 0860-8229
www.metrology.wat.edu.pl

M&MS

APPLICATION OF WAVELET EXPONENTIAL WINDOW DENOISING AND DYNAMIC UNCERTAINTY IN ACOUSTIC EMISSION

Lide Fang[1)], Jianzhang Sun[4)], Meng Zheng[1)], Qiaoqiao Zeng[2)], Fang Dong[1)], Yue Feng[3)]

1) Hebei University, School of Quality and Technical Supervision, Hebei, Baoding, 071000, China
(✉ *dongfang1023@163.com*)
2) Hubei Huangshi Institute of Measurement and Testing, Huangshi, Hubei, Hubei, 435000, China
3) School of Electronic Information Engineering, Langfang Normal University, Langfang, 065000, China
4) Institute of Metrology of Hebei Province, 050200, China

Abstract

The gas-liquid two-phase acoustic emission (AE) signal contains rich flow information, but it is also accompanied by a large number of interference signals. To accurately extract the characteristics of gas-liquid two-phase flow, the removal of interference signals is very important. In this paper, AE technology is used to detect the signal of gas-liquid two-phase flow in a vertical pipeline. The support degree of the sensor is checked by the trust function to confirm the consistency of the sensor and eliminate wrong data. The decomposition level of the wavelet base and wavelet transform is determined by four parameters such as the signal-to-noise ratio. By comparing the wavelet exponential window smoothing method and the wavelet soft threshold method, the wavelet exponential window smoothing method which is more suitable for the denoising effect is selected, and the real-time denoising effect is evaluated by using the measurement dynamic uncertainty theory. The results show that the wavelet exponential window denoising method improves the signal-to-noise ratio, reduces the energy leakage during denoising, and significantly improves the pseudo-Gibbs phenomenon, while dynamic uncertainty can effectively evaluate the denoising effect of AE signals.

Keywords: acoustic emission, dynamic uncertainty, gas-liquid two-phase flow, wavelet transform.

1. Introduction

Acoustic emission technology, as a new means of measurement, can be used to evaluate the state of materials or detect the integrity of structures by detecting and analysing the tiny sound waves generated by materials or systems under stress. This technology is widely used in various industries because of its non-invasive, real-time monitoring ability, and high sensitivity [1–5]. Also, some studies focus on AE signal characteristics [6–9] and cover AE signal analysis [10–12]. With the progress of science and technology and the deepening of research, acoustic emission technology has been further expanded in other application fields, one of which is the research

Article history: received November 29, 2023; revised June 3, 2024; accepted July 23, 2024; available online September 18, 2024.

and application in the field of multiphase flow [13–21]. Many efforts have been made in the field of gas-liquid two-phase flow in multiphase flow. Li *et al.* [22] designed a multi-sensor based on near-infrared, an AE sensor, and a throat tube and applied it to gas-liquid two-phase flow, proposing a new gas volume fraction model. Diao, Xu *et al.* [23] proposed a variational mode decomposition method for detecting the existence and importance of leakage in fluid pipelines by improving signal denoising on the basis of adequate signal processing of AE signals.

One of the main challenges of AE signal analysis is the existence of noise. In the actual acquisition process, there are different mechanical and electromagnetic noises in the environment. If the existing noise cannot be effectively eliminated, the accuracy of the signal is affected, thus in recent years, researchers have employed various denoising techniques for processing acoustic emission signals. Liu, Tong *et al.* [24] utilized the AE-WPD method for acoustic emission denoising. Yu, Aiping *et al.* [25] applied SOM neural networks for machine learning-based acoustic emission denoising, achieving significantly improved filtering effects compared to hardware-based filters. Kim, Jinki *et al.* [26] proposed an online acoustic emission signal den[ising strategy using *stochastic resonance* (SR) in bistable system arrays. These studies have facilitated the extraction of useful information by effectively denoising acoustic emission signals. Therefore, the successful application of AE technology in gas-liquid two-phase flow is determined by how to extract and remove redundant interference information and how to identify useful information from AE signals.

Based on this, the present study adopts the method of combining wavelet transform and the exponential window smoothing method to carry out AE signal denoising processing and combines the uncertainty and diversity of AE signals. In this paper, the idea of dynamic uncertainty is innovatively incorporated into the evaluation of AE denoising effect, and it is concluded that the noise removal method using the wavelet exponential window smoothing method improves the signal-to-noise ratio compared with the noise removal method using wavelet soft thresholding, and dynamic uncertainty can be used to evaluate the noise removal effect of AE signals.

The remaining parts of this paper are organized as follows. In Section 2, the theoretical foundation of this paper is introduced. In Section 3, we establish the experimental system for the acoustic emission experiments. In Section 4, we process and analyse the experimental data, demonstrating the superiority of the wavelet thresholding method for denoising. In Section 5, we analyse the dynamic uncertainty of the collected data, accurately reflecting the real-time capabilities after denoising, and confirm the feasibility of using dynamic uncertainty as a metric for evaluating the effectiveness of the denoising process.

2. Theoretical basis

The basic model of exponential smoothing is as follows:

$$s_{k,t}(t) = af(t) + (1-a)s_{k,t}(t-1) \tag{1}$$

where $f(t)$ is the number of advance periods predicted, a is the weight coefficient and the range is from 0 to 1.

The parameters are expressed as follows:

$$\begin{cases} {s_{k,t}}^{(1)} = af(t) + (1-a)s_{k,t}(t-1)^{(1)} \\ {s_{k,t}}^{(2)} = a{s_{k,t}}^{(1)} + (1-a)s_{k,t}(t-1)^{(2)} \\ {s_{k,t}}^{(3)} = a{s_{k,t}}^{(2)} + (1-a)s_{k,t}(t-1)^{(3)} \end{cases}, \tag{2}$$

where ${s_{k,t}}^{(1)}$, ${s_{k,t}}^{(2)}$, $s_{k,t}^{(3)}$ are the first, the second, the third exponential smoothing values corresponding to the t-th.

$$f_{t+m} = A_{k,t} + B_{k,t}m + \frac{1}{2}C_{k,t}m^2, \qquad k = 1, 2, 3, \ldots,$$

$$\begin{cases} A_{k,t} = 3{s_{k,t}}^{(1)} - 3{s_{k,t}}^{(2)} + {s_{k,t}}^{(3)} \\ B_{k,t} = \dfrac{a_{k,t}}{2(1-a_{k,t})}[(6-5a_{k,t}){s_{k,t}}^{(1)} - (10-8a_{k,t})s_{k,t}^{(2)} + (4-3a_{k,t}){s_{k,t}}^{(3)}] \\ C_{k,t} = \dfrac{a_{k,t}}{2(1-a_{k,t})}({s_{k,t}}^{(1)} - 2{s_{k,t}}^{(2)} + {s_{k,t}}^{(3)}) \end{cases}, \tag{3}$$

where $A_{k,t}$, $B_{k,t}$, $C_{k,t}$ is the t-th prediction coefficient, and m is the forecast lead time coefficient.

Because of constant updating of the forecast data, the exponential smoothing method is widely used in the economy. The model provides a good predictive effect on the data with a certain trend, non-linearity, multi-factors and long-term. Data have the same characteristics in flow noise, so exponential smoothing can be considered the best method to predict and update data in flow noise. According to the wavelet theory, flow noise signal can be divided into two parts, one is composed of wavelet function and the other is composed of the scale function.

$$f(t) = \sum_{j=1}^{n}\sum_{k\in z} d_k^j \Psi_{j,k}(t) + \sum_{k\in z} c_k^n \phi_{j,k}(t), \tag{4}$$

where n is the number of the decomposition level, d_k^j is the k component of the j level, c_k^N is the decomposition scale coefficient, $\Psi_{j,k}(t)$ is a basic wavelet function and $\phi_{j,k}(t)$ is the scaling function. In this paper, the wavelet function is a db function (compactly supported orthogonal wavelet), and the scaling function is the exponential window smoothing function [27].

The binary discrete wavelet function generated by the wavelet generating function is expressed as:

$$\Psi_{j,k}(t) = 2^{-j/2}\Psi(2^{-j} - k), \tag{5}$$

with $\Psi(t)$ being a band-pass filter, in which the db function of the wavelet function is expressed as:

$$\Psi_{j,k}(t) = \sum_{k=0}^{n-1} C_k^{n+k+1} Y^k \tag{6}$$

The essential part of the scaling function is the exponential smoothing function. The time domain varies sharply and a narrow time window is adopted for non-stationary signals. The frequency domain window is narrow and the temporal resolution is improved. This is stated as:

$$|\hat{\phi}(w)|^2 = \sum_{j=1}^{\infty} |\hat{\phi}(2^{jw})|^2, \tag{7}$$

$$\text{Ø}_{j,k}(t) = aY(t) + (1-a)\text{Ø}_{j,k}(t-1). \tag{8}$$

The basic wavelet function is used to decompose and the exponential window smoothing function is used to predict and update the signal [28, 29]. The reconstructed information can then be obtained by substituting the updated coefficients into (4).

$$f(t) = \sum_{j=1}^{n}\sum_{k\in z} d_k^j \left(\sum_{k=0}^{n-1} C_k^{n+k+1} Y^k\right) + \sum_{k\in z} aY(t) + (1-a)\text{Ø}_{j,k}(t-1). \tag{9}$$

3. Construction of the acoustic emission experimental system

Acoustic emission technology uses a piezoelectric probe mounted on the surface of a material or component to receive elastic waves and convert them into electrical signals. Then the subsequent circuit to process is used and the detected electrical signal is displayed from which the internal conditions of materials or components are obtained.

3.1. Construction of the experimental system

The experiments were conducted using the multi-phase flow experimental platform of Hebei University. Gas-liquid two-phase flow noise was acquired using the sensor highway III AE instrument (manufactured by the American Physical Acoustics). The sampling rate was set at 5MHz, with a total of 1048500 sampling points. The experimental probe's mounting position and the principle behind acquiring flow noise are illustrated in Fig. 1. P1, P2, P3, and P4 correspond to Sensors 1, 2, 3, and 4 respectively. In the presence of two-phase flow in the pipeline, interactions between liquid-liquid interfaces, gas-liquid interfaces, and the gas-liquid wall generate *acoustic emission* (AE) signals that reflect the underlying mechanisms governing two-phase flow behaviour. Utilizing the piezoelectric effect within the AE sensor probe, these two-phase flow noise signals are converted into electrical signals. Subsequently, weak electrical signals are amplified through the utilization of a sensor highway III acquisition device which records and displays them via a signal acquisition system before converting analogue signals into digital ones for transmission to a desktop computer.

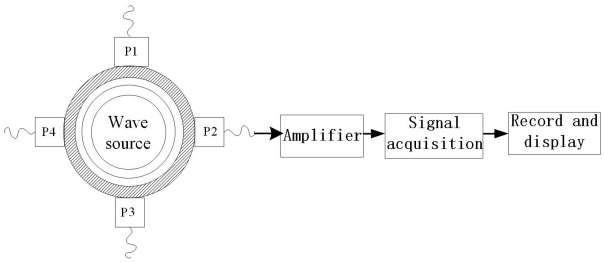

Fig. 1. Schematic diagram of flow noise acquisition.

3.2. Experimental Test

To study the de-noising method, an AE detection system is used to measure the static and flow conditions of single-phase water.

The actual test system is shown in Fig. 2.

Fig. 2. Actual test system.

4. Data analysis

The principle of wavelet transforms and exponential window smoothing is used to evaluate the dynamic uncertainty of noise signal in this paper. Firstly, the data from each sensor probe is read in, and the degree of support between sensors is determined by the trust function. When each sensor meets the support level, the data is retained; when it does not meet the requirements, the data is discarded. Then, the wavelet basis function and the decomposition level are confirmed, and the signal-to-noise ratio is used as the de-noising effect. The basis of evaluation is to ensure that data information is not lost. This is done by determining the input sensor data, setting the wavelet analysis de-noising parameters, and then starting wavelet exponential window smoothing de-noising. The effectiveness of de-noising is evaluated by dynamic uncertainty.

4.1. Sensor detection

The measurement data of unstable performance cannot be determined for sensors. Jia et al used confidence distance to compare the measured data and to check the validity of the sensor [30]. While Akhoundi used a confidence function (2σ) to express the trust between sensors [31].

The confidence function of 2σ is used to express the trust degree among sensors in this paper. The calculation formula is as follows:

$$d_{ij} = \exp^{[-\frac{1}{2}\frac{(x_i - x_j)^2}{(2\sigma_i)^2}]}, \tag{10}$$

where x_i and x_j are measured values and σ_i is deviation.

The obtained data are then solved to obtain the variance of the support degree of the sensor. Specific values are shown in Table 1.

Table 1. Support level solution parameter (v).

Serial number	**1**	**2**	**3**	**4**
Measured value	0.0040	0.0040	0.0011	0.0005
σ^2 variance (e–7)	0.0103	0.0045	0.0047	0.0076

The data in Table 1 is taken into the 2σ confidence function to calculate the trust matrix.

$$d_{ij} = \begin{bmatrix} 1.0000 & 0.9811 & 0.0028 & 0.9839 \\ 0.9577 & 1.0000 & 0.0000 & 0.8522 \\ 0.0000 & 0.0000 & 1.0000 & 0.0000 \\ 0.9783 & 0.9091 & 0.0008 & 1.0000 \end{bmatrix} \tag{11}$$

From the trust matrix, it is apparent that the mutual support degree between Sensor 1 and Sensor 2 is high, while the support degree of Sensor 4 is relatively low, and the support degree of Sensor 3 is zero. Therefore, it can be determined that Sensor 3 is the fault sensor.

4.2. Selection of Wavelet Functions

For the choice of a wavelet function, the property of the wavelet function is theoretically analysed, and the signal-to-noise ratio of the wavelet function is compared from the angle of measurement value.

By comparing the orthogonality, biorthogonality, compact support, symmetry and regularity of five wavelets, the properties of the continuous wavelet transform, and discrete wavelet transform, it can be concluded that the Haar function has no regularity, the dB function has no symmetry, approximate regularity, bior's property has no orthogonality and regularity, coif has approximate symmetry. The db function has no regularity, and sym has approximate symmetry and no regularity. The specific properties are shown in Table 2.

Table 2. Comparison of wavelet properties

Function	Haar	db	bior	coif	sym
Orthogonality	✓	✓	×	✓	✓
Biorthogonality	✓	✓	✓	✓	✓
Compact support	✓	✓	✓	✓	✓
Symmetry	✓	×	✓	–	–
Regularity	×	–	×	×	×

From the theoretical point of view, the flow noise signal measured by the AE system is continuous. To satisfy the signal integrity as much as possible, three wavelets, db, sym and coif, are selected.

Using coif, rbio, Haar, birothogonal, db, symlets and dmey as the wavelet generating functions, and based on the default decomposition level of five layers, the soft threshold processing method is used to de-noise, after which the corresponding data is obtained.

The *root means square error* (RMSE), *signal-to-noise ratio* (SNR), smoothness index (r) and correlation coefficient (R) of the evaluation methods of wavelet de-noising quality have been previously used [32–35] as the evaluation indexes for determining the superiority of wavelet.

The root means square error:

$$\mathrm{RMSE} = \sqrt{\frac{1}{n}\sum_{i=1}^{n}[f(i) - \hat{f}(i)]^2}, \tag{12}$$

The signal-to-noise ratio (SNR):

$$\mathrm{SNR} = 10 \times \log \frac{\sum_{i=1}^{n}[f(i)]^2}{\sum_{i=1}^{n}[f(i) - \hat{f}(i)]^2}, \tag{13}$$

The smoothness index (r):

$$r = \frac{\sum_{i=1}^{n-1}[\hat{f}(i+1) - \hat{f}(i)]^2}{\sum_{i=1}^{n-1}[\hat{f}(i+1) - f(i)]^2}, \tag{14}$$

The correlation coefficient (R):

$$R = \frac{\mathrm{COV}(f(i), \hat{f}(i))}{\sigma_{f(i)}\sigma_{\hat{f}(i)}}, \tag{15}$$

where n is the length, $f(i)$ is the original signal, and $\hat{f}(i)$ is the data obtained after de-noising.

The RMSE is close to zero, indicating a better de-noising effect. SNR is the ratio of energy to noise energy of data signals, and the criterion is that the larger the SNR is, the better.

Metrol. Meas. Syst., Vol. 31 (2024), No. 4, pp. 637–655
DOI: 10.24425/mms.2024.152045

When the cross-correlation number is enlarged by 10 times, the evaluation criterion is that the correlation number is closer to 10, the better. The smoothness index can reflect the smoothness of the reconstructed signal. Because the original signal has a good correlation, therefore, smoothness is an important index to judge the effect of anomaly data processing. The smaller the smoothness, the better the effect of anomaly data processing.

Using the wavelet generating function coiflets, rbio, Haar, birothogonal, db, symlets, dmey in the wavelet is based on the default decomposition level of the five, applying the soft-threshold processing method to de-noise.

From the Fig. 3, it can be seeing that the peak values of RMSE, SNR, R and r are reflected in bior and rbio functions, while coif, db, fk and sym functions are relatively stable. Coif, db and sym are three kinds of wavelet basis functions, and the evaluation criteria of these three kinds of wavelet basis functions are compared again.

a) RMSE change curve

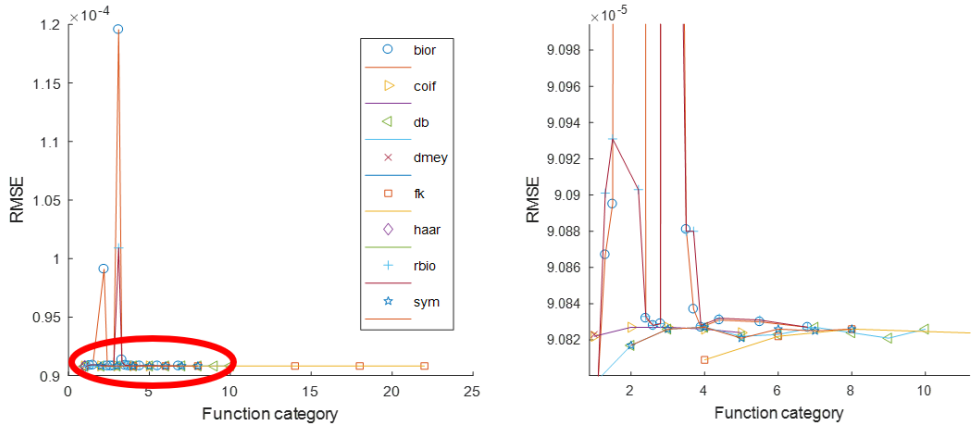

b) SNR change curve

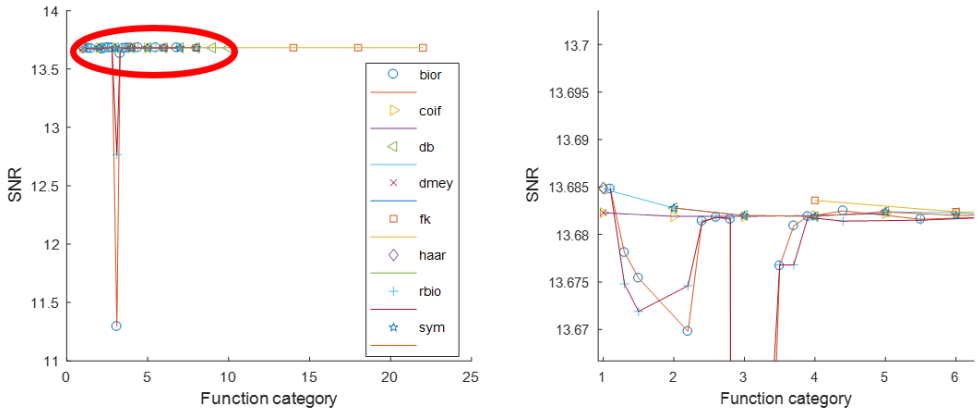

Fig. 3. Coefficient change diagram.

c) R change curve

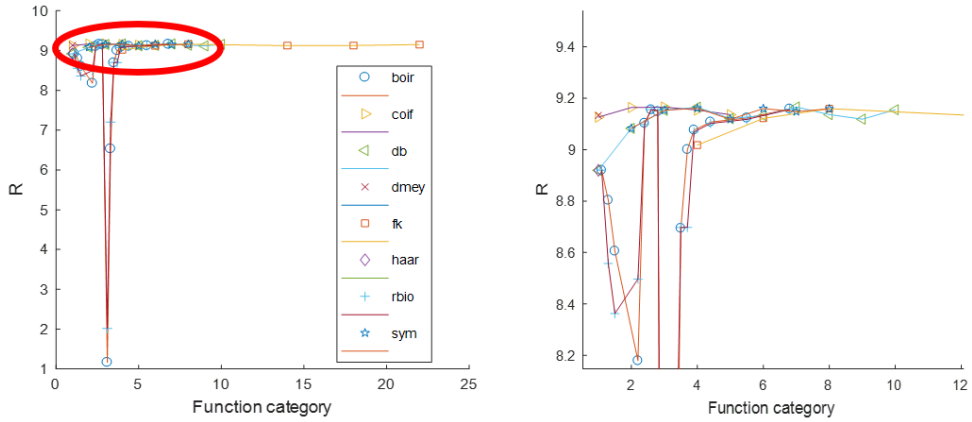

d) r change curve

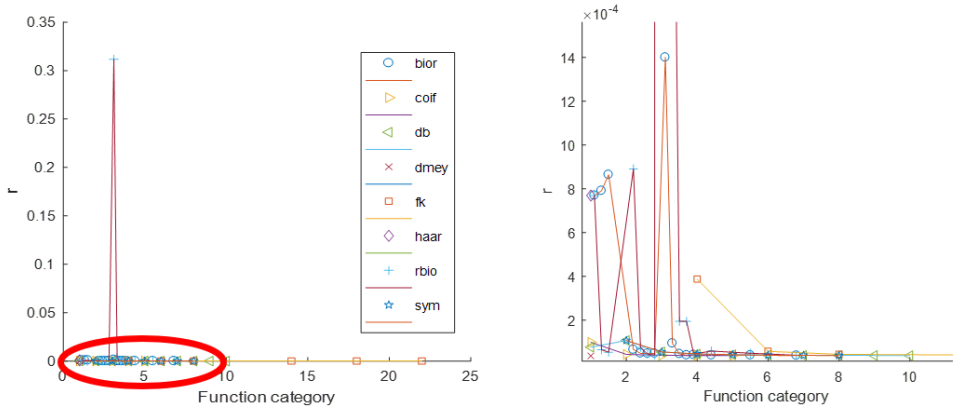

Fig. 3. [cont.]

As can be seen in Table 3, db1 demonstrated the lowest RMSE, the highest SNR, a cross-correlation coefficient R close to 10, and a satisfactory smoothness index r. In comparison to other wavelet basis functions, signals processed with the db basis function exhibited superior overall performance.

Table 3. Evaluation index.

Function	RMSE	SNR	R	r
coif1	0.90822×10^{-4}	13.6823	9.1264	0.98969×10^{-4}
coif2	0.90827×10^{-4}	13.6819	9.1641	0.441350×10^{-4}
coif3	0.90827×10^{-4}	13.6819	9.1658	0.396330×10^{-4}
coif4	0.90826×10^{-4}	13.6820	9.1543	0.386223×10^{-4}
coif5	0.90824×10^{-4}	13.6822	9.1362	0.384440×10^{-4}

Table 3. [cont.]

Function	RMSE	SNR	*R*	*r*
db1	0.90796×10^{-4}	13.6848	9.1699	0.769570×10^{-4}
db2	0.90817×10^{-4}	13.6828	9.0830	1.072400×10^{-4}
db3	0.90826×10^{-4}	13.6820	9.1533	0.552710×10^{-4}
db4	0.90827×10^{-4}	13.6819	9.1651	0.451070×10^{-4}
db5	0.90822×10^{-4}	13.6824	9.1212	0.426450×10^{-4}
db6	0.90823×10^{-4}	13.6823	9.1326	0.407490×10^{-4}
db7	0.90827×10^{-4}	13.6819	9.1660	0.391100×10^{-4}
db8	0.90824×10^{-4}	13.6822	9.1366	0.392480×10^{-4}
db9	0.90821×10^{-4}	13.6824	9.1188	0.392700×10^{-4}
db10	0.90826×10^{-4}	13.6820	9.1553	0.381420×10^{-4}
sym2	0.90817×10^{-4}	13.6828	9.0830	1.072400×10^{-4}
sym3	0.90826×10^{-4}	13.6820	9.1533	0.552710×10^{-4}
sym4	0.90827×10^{-4}	13.6819	9.1614	0.460940×10^{-4}
sym5	0.90821×10^{-4}	13.6824	9.1181	0.427190×10^{-4}
sym6	0.90826×10^{-4}	13.6820	9.1597	0.401010×10^{-4}
sym7	0.90825×10^{-4}	13.6821	9.1478	0.395890×10^{-4}
sym8	0.90826×10^{-4}	13.6819	9.1591	0.386670×10^{-4}

4.3. Selection of wavelet decomposition layers

With db1 as the wavelet function, the soft threshold method is used for wavelet de-noising. After data reconstruction, the de-noised data is derived, and the signal-to-noise ratio is used as an index for selecting the number of wavelet decomposition layers.

In the case of different layers of wavelet basis function db1, the processed data and the original signal data are substituted into the signal-to-noise ratio formula to obtain the variation of the signal-to-noise ratio of db1 with the increase of the number of decomposition layers it goes through. It can be seen from Table 4 that the signal-to-noise ratio shows a gradual decreasing trend

Table 4. Evaluation index after db1 layering.

Function	RMSE	SNR	*R*	*r*
db1-1	0.65278×10^{-4}	16.5508	0.6997	0.571300000000
db1-2	0.83772×10^{-4}	14.3842	0.3993	0.107200000000
db1-3	0.88770×10^{-4}	13.8809	0.237	0.014800000000
db1-4	0.90111×10^{-4}	13.7506	0.1656	0.003800000000
db1-5	0.90796×10^{-4}	13.6848	0.1121	0.000769570000
db1-6	0.91074×10^{-4}	13.6583	0.0807	0.000201920000
db1-7	0.91221×10^{-4}	13.6443	0.0576	0.000050340000
db1-8	0.91295×10^{-4}	13.6373	0.0413	0.000012812000
db1-9	0.91332×10^{-4}	13.6337	0.0298	0.000003146600
db1-10	0.91350×10^{-4}	13.6320	0.0223	0.000000852220

with the increase of the number of layers. The signal-to-noise ratio data changes greatly from the first layer to the fourth layer and tends to be stable from the sixth layer to the twelfth layer.

In the case of AE noise, disturbance noise mainly exists in low-frequency signals, and the main flow noise exists in high-frequency signals. In wavelet de-noising, with the increase of decomposition layers, the de-noising of low-frequency signals is further optimized. At the same time, from the point of view of data calculation, the decomposition level to the 6th level can be seen as the best. Therefore, it can be concluded that the optimal number of wavelet decomposition layers is 6. Finally, it is determined that the wavelet function used for de-noising is db1, and the decomposition layer is 6 layers.

4.4. Wavelet exponential smoothing method for de-noising

For the data collected by AE, it has the characteristics of real-time and a large sample size. In the process of data processing, measurement and calculation of a period fragment is usually performed. When the time fragment is intercepted, energy leakage will occur in the signal. In addition, when wavelet analysis is carried out, the time domain is transformed into the frequency domain, and energy leakage is also generated. When FFT transform is applied, there will be a hurdle effect. These two energies cannot cancel each other. In this case, when FFT is performed with the help of window functions, there will be a gradual and continuous reduction of energy leakage and fence effect.

In contrast to Table 4, for different window functions, using mean square deviation and signal-to-noise ratio as the selection conditions, it is concluded that the wavelet exponential window smoothing method has the smallest RMSE and the largest SNR, which is suitable for de-noising, so the window smoothing function is selected.

Table 5. Comparison of parameters.

Method	RMSE	SNR
Exponential	7.7181e-09	13.9567
Gaussian	8.2179e-09	13.6842
Box	8.0778e-09	13.7589
Lowess	7.9921e-09	13.8029
Sgolay	8.5919e-09	13.4927
Medfilt	8.3580e-09	13.6085

As shown in Table 5, the six-window smoothing functions, exponential window function, Gaussian window function, box window function, Lowess window function, Savitzky–Golay filter window function and median window function are evaluated in the process of window function selection. To reduce energy leakage and the pseudo-Gibbs (the pseudo-Gibbs effect) [36, 37], according to the properties of mean square deviation and signal-to-noise ratio, the smaller the mean square deviation, the greater the signal-to-noise ratio, which shows the better de-noising effect. By looking at Table 5 above, it can be concluded that, amongst all the six window methods, the exponential sliding window function method has the smallest mean square deviation and the largest signal-to-noise ratio. Therefore, the exponential sliding window method is used to further reduce energy leakage and fence effect.

The db1 is chosen as the wavelet function, and the decomposition level is 6 layers. At the same time, the exponential window smoothing method in soft threshold is used for de-noising. Under

Metrol. Meas. Syst., Vol. 31 (2024), No. 4, pp. 637–655
DOI: 10.24425/mms.2024.152045

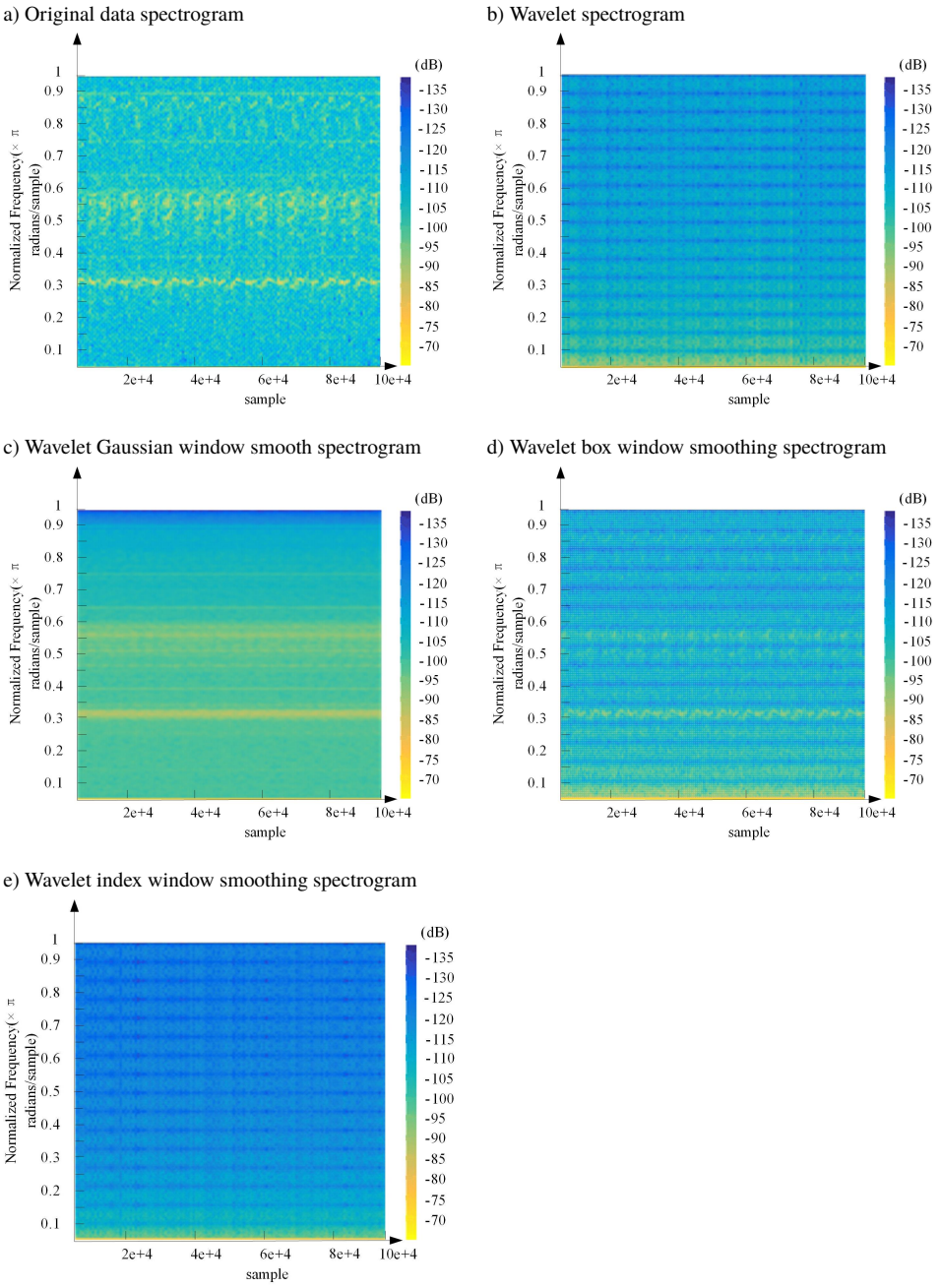

Fig. 4. Sonograms for different methods.

different de-noising conditions of wavelet de-noising and wavelet exponential window smoothing, the data collected by Sensors 1, 2 and 4 with a support degree are compared by the RMSE and SNR the results which are shown in Table 6.

From the data in Table 6, it can be seen that the growth rate of signal-to-noise ratio of Probe 1 is 139.31%, Probe 2 is 104.02%, and Probe 4 is 88.13%.

Table 6. Comparison of parameters.

Probe	Parameter	Method 1	Method 2
1	RMSE	8.2665e-09	9.8950e-11
	SNR	13.6585	32.6864
2	RMSE	3.8953e-09	8.3954e-11
	SNR	15.9126	32.4649
4	RMSE	3.3811e-09	8.1452e-11
	SNR	18.2882	34.4049

The original data and the processed data are respectively applied to chaos and the resulting image of 3D is shown in Fig. 5.

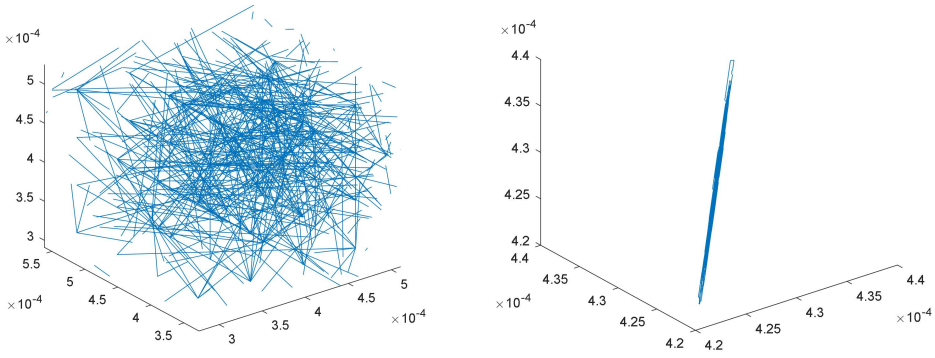

a) Image obtained by applying initial data to chaos. b) Image obtained by applying processed data to chaos.

Fig. 5. Three-dimensional image applied to a chaotic system.

In Fig. 5, numerous sub-chaotic systems are visible without denoising, illustrating the multidimensional chaotic nature of signals before and after denoising. Before denoising, the state appears chaotic and disordered, making it challenging to extract effective signals. However, upon applying the wavelet exponential window smoothing method to denoising, the resulting images become notably clearer, with a significant reduction in chaos. This enhances multidimensional consistency, facilitating the extraction of effective signals. The denoising efficacy demonstrated aligns with the findings in Table 6, which also show the results of utilizing the wavelet exponential window smoothing method. Fig. 5 vividly illustrates the denoising effectiveness of this method through the chaos plots.

In Fig. 4, representing the sonograms for different methods, various colours are used to denote high and low-frequency signals, transitioning from low to high frequencies. In the original signal, low-frequency signals may be embedded within high-frequency ones. Since the test conditions involve pure water at rest, removing low-frequency signals is necessary for data processing and denoising. Initially, low-frequency signals are scattered within the original noisy signal. After wavelet soft-threshold denoising, prominent low-frequency signals are removed, yet there is

a noticeable energy leakage between decomposed signals. Wavelet-Gaussian window smoothing denoising reduces the energy leakage but does not effectively handle low-frequency noise signals. Therefore, the wavelet box smoothing denoising method is employed to eliminate low-frequency noise. Though slightly inferior to wavelet soft-threshold denoising in preserving frequency signals, it minimizes energy repetition between signal layers. Notably, the wavelet exponential window smoothing denoising method effectively removes low-frequency signals and reduces energy leakage, yielding promising results.

5. Analysis of dynamic uncertainty

For AE signal denoising, wavelet transform is a common technique, but in the process of wavelet decomposition and reconstruction, there will be an energy leakage and the fence effect at the critical truncation. Therefore, the evaluation of the noise removal effect is a key factor affecting the analysis of gas-liquid two-phase flow. By summarizing the previous experience, there are six kinds of quality evaluation of wavelet noise removal:

- RMSE is used for evaluation [34];
- Using the correlation number to evaluate [35];
- The SNR is used as the evaluation standard [36]

and the smoothness (r), which can reflect the smoothness of the reconstructed signal, is used as the evaluation index [37]. The correlation coefficients were calculated by equal measures and added together, and the overall evaluation method was used [38]. The denoising quality of wavelet can be effectively evaluated by using the uncertainty of the estimation of the signal reconstruction interval [39]. Here, we propose a new method: dynamic uncertainty is applied to the evaluation of noise signal.

5.1. Theoretical Analysis of Wavelet Signal Evaluation Based on Dynamic Uncertainty

Usually, there are main parameters to evaluate de-noising signal: *mean absolute error* (MAE), *mean square error* (MSE), RMSE, SNR and *peak signal-to-noise ratio* (PSNR). However, the energy leakage phenomenon is mainly manifested in the process of wavelet decomposition. If only the integrity analysis is carried out, the shortcomings of the above denoising methods in the intermediate process cannot be reflected. Compared with static measurement, dynamic data collected by AE devices has the characteristics of real-time, dynamic, and random, and its influencing factors are more complex. In addition, the dynamic measurement itself has the advantage of improving the accuracy of digital calculation and the reliability of measurement results. Therefore, the dynamic uncertainty method should be selected to evaluate the dynamic denoising performance.

In order to meet the requirement of real-time evaluation in uncertainty analysis of deterministic components, and considering factors such as variance, efficiency, and robustness, the least squares fitting method in uncertainty theory was adopted.

Step 1: subtracting the deterministic component from the original data to obtain a residual.

$$v(i) = x(i) - x_c(i) \tag{16}$$

where $x(i)$ is the original data, $x_c(i)$ is the deterministic component.

Step 2: The standard deviation of unit weight is taken:

$$\mu(i) = \sqrt{\frac{\sum_{i=1}^{n} v^2(i)}{n-2}}. \tag{17}$$

Step 3: The uncertainty of deterministic components of i point is obtained:

$$s_c(i) = \left\{ \frac{\mu^2(i)}{n s_i(i)} \left(\sum t_i^2 + t_i^2 n - 2t_i \sum t_i \right) \right\}^2. \tag{18}$$

where n is the length of fitting data and i is the corresponding time of fitting.

$$s_i(i) = \sum t_i^2 - \frac{1}{n} \left(\sum t_i \right)^2, \tag{19}$$

$$Y(i) = \omega_{p1} Y(i-1) + \omega_{p2} Y(i-2) + \cdots + \omega_{pp} Y(i-p) + \varepsilon(i), \tag{20}$$

where p is the order, ω_{pi} is the estimated parameter, $\varepsilon(i)$ is the error term for stochastic components.

So, the final randomness uncertainty can be expressed as:

$$\varepsilon(i) = Y(i) - \omega_{p1} Y(i-1) - \omega_{p2} Y(i-2) - \cdots - \omega_{pp} Y(i-p), \tag{21}$$

$$s_r(i) = \varepsilon(i) \tag{22}$$

Step 4: the dynamic uncertainty is obtained:

$$s(i) = \sqrt{s_c^2(i) + s_r^2(i)}. \tag{23}$$

5.2. Data comparison

The acoustic emission signal acquisition system has 1048500 sampling points and, in order to clearly highlight the de-noising effect, 90 sampling points were randomly intercepted. Fig. 6 shows a comparison of the original data and noise reduction data from each sensor.

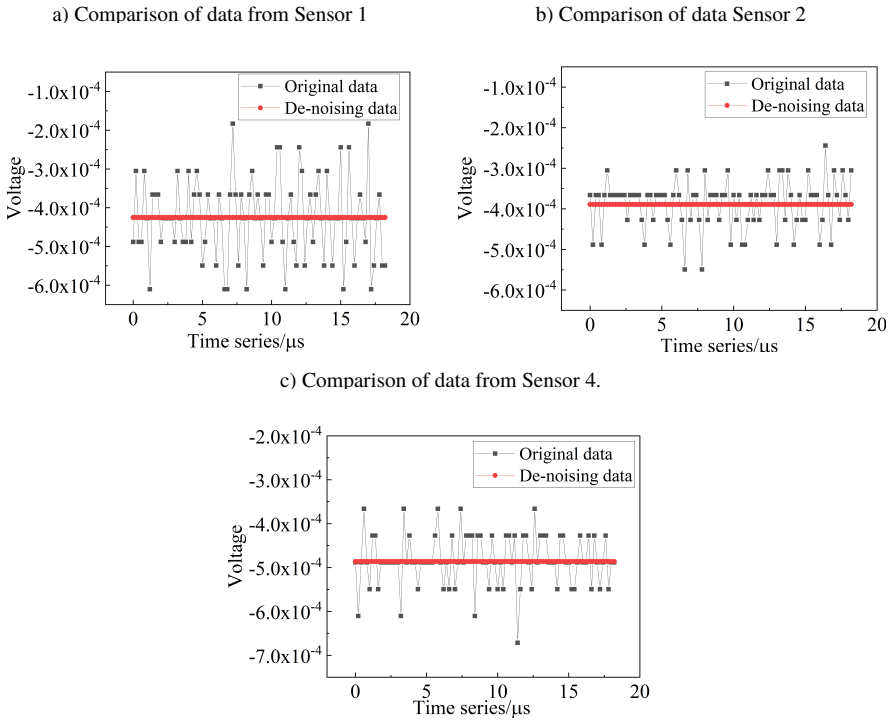

Fig. 6. Comparison of sensor data.

Metrol. Meas. Syst., Vol. 31 (2024), No. 4, pp. 637–655
DOI: 10.24425/mms.2024.152045

Since the original signal contains noise, the useful signal was obscured by it. Comparing the raw data with the denoised data of various sensors, it is evident from Fig. 6 that the signal fluctuation range of the raw data is large, between $_6 \times 10^{-4}$ V to -3×10^{-4} V. This substantial fluctuation indicates that the sensor's raw data contains noise signals, making it difficult to distinguish the useful signal and affecting the accuracy and reliability of data analysis.

However, the signal processed through the wavelet index window smoothing method tends to stabilize with a smaller fluctuation amplitude, stabilizing at around -4×10^{-4} V with almost no fluctuation, significantly restoring the signal's authenticity. The results demonstrate that the wavelet index window smoothing method can effectively remove noise from useful signals, proving the superiority of the wavelet index window smoothing method when used for denoising.

5.3. Comparison of dynamic uncertainty of data

Figure 7 shows the dynamic uncertainty obtained for Sensors 1 and 4 using both wavelet soft thresholding for noise reduction and wavelet index window smoothing methods. It can be observed that in the 10~100 range, wavelet soft thresholding introduces additional discretization error, leading to a significant energy leakage and the pseudo-Gibbs phenomenon. In contrast, wavelet index window smoothing for noise reduction displays relatively stable performance in the 10~100 range without significant fluctuations, indicating no obvious energy leakage or pseudo-Gibbs phenomena.

a) Smooth dynamic uncertainty for Sensor 1.

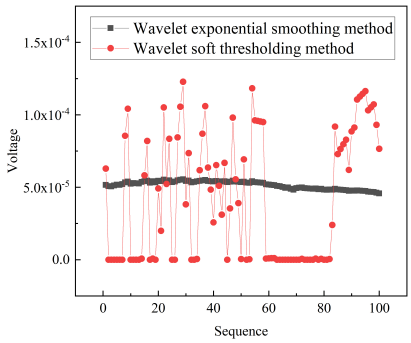

b) Smooth dynamic uncertainty for Sensor 4.

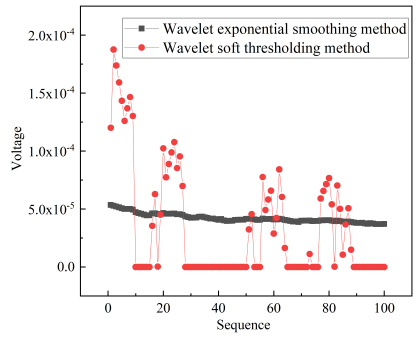

Fig. 7. Comparison of the smooth dynamic uncertainty of No. 1 and No. 4 wavelet exponential windows.

Regarding the dynamic uncertainty, through the formulas (16)–(23) in Section 5.1, it can be calculated that the dynamic uncertainty reduction for Sensor 1 using wavelet index window denoising compared to wavelet soft thresholding denoising is 47.9%, and for Sensor 4, it is 52.3%. This indicates that the signal fidelity through wavelet index window denoising is better, with lower noise and error, the signal's fluctuation amplitude is smaller, displaying more stable and reliable performance, and better denoising effects. Smaller amplitude changes and lower noise lead to high-quality signal performance indicated by minimal energy leakage. Similarly, when dynamic uncertainty is low, the signal processing within the window application and Fourier transform process is more precise, thereby improving the pseudo-Gibbs phenomenon.

6. Conclusions

The de-noising analysis is an important step in gas-liquid two-phase flow AE signal processing. In this paper, AE data are obtained by experiment and the wavelet exponential window smoothing method is used in the de-noising analysis. Dynamic uncertainty is used to evaluate the de-noising effect. Using the trust degree function to test the degree of support of the sensor can enhance the credibility of the experimental data. Based on the growth rate of the SNR of the probes, it is apparent that the de-noising method using the wavelet exponent window smoothing method improves the SNR compared with wavelet de-noising. Correct reflection of wavelet exponential window de-noising method can reduce energy leakage in the process of de-noising, and the pseudo-Gibbs phenomenon has been significantly improved. Based on the analysis of the experimental results, it can be concluded that the proposed method is feasible and can be used for de-noising analysis of gas-liquid two-phase flow AE signal processing.

Acknowledgements

The study was supported by Post-Graduate Innovation Fund Project of the Hebei Province (CXZZBS 2023026), the Science and Technology Project of the Hebei Education Department (QN2023077), the National Natural Science Foundation of China (62173122), the Key Project of Natural Science Foundation of Hebei Province (F2021201031), Hebei Provincial Postgraduate Demonstration Course Project (KCJSX2021009).

References

[1] Feng, Q., Yongzhong, B., Dingrong, Q., & Wenwu, C. (2022). Acoustic mechanism and characteristics of corrosion bubble rupture. *Insight - Non-Destructive Testing and Condition Monitoring*, *64*(2), 99–107. https://doi.org/10.1784/insi.2022.64.2.99

[2] Wang, G., Song, L. B., Liu, X. Q., Bao, C. Y., Lin, M. Q., & Liu, G. J. (2022). Shear Fracture Mechanical Properties and Acoustic Emission Characteristics of Discontinuous Jointed Granite. *Rock and Soil Mechanics*, *43*(6), 1533–1545. https://doi.org/10.16285/j.rsm.2021.2120

[3] Han, C., Yang, G., Wang, J., & Guo, X. (2020). The research on propagation characteristics of acoustic emission signals in stiffened plates based on the multipath propagation model. *Ultrasonics*, *108*, 106177. https://doi.org/10.1016/j.ultras.2020.106177

[4] Witos, F., Opilski, Z., Szerszeń, G., & Setkiewicz, M. (2019). The 8AE-PD computer measurement system for registration and analysis of acoustic emission signals generated by partial discharges in oil power transformers. *Metrology and Measurement Systems*, 403–418. https://doi.org/10.24425/mms.2019.128355

[5] Mao, F., Fang, S., Li, M., Huang, C., Deng, T., Zhao, Y., & Qin, G. (2022). Study on Attenuation Characteristics of Acoustic Emission Signals with Different Frequencies in Wood. *Sensors*, *22*(16), 5991. https://doi.org/10.3390/s22165991

[6] Mukherjee, A., & Banerjee, A. (2020). Analysis of Acoustic Emission Signal for Crack Detection and Distance Measurement on Steel Structure. *Acoustics Australia*, *49*(1), 133–149. https://doi.org/10.1007/s40857-020-00208-z

[7] Fernández, A., Rescalvo, F. J., Cruz, A., Abarkane, C., & Santiago, J. M. (2019). Acoustic emission analysis of raw bamboo subjected to tensile tests. *Mechanics of Advanced Materials and Structures*, *28*(13), 1389–1397. https://doi.org/10.1080/15376494.2019.1675105

[8] Świt, G., Dzioba, I., Adamczak-Bugno, A., & Krampikowska, A. (2022). Identification of the Fracture Process in Gas Pipeline Steel Based on the Analysis of AE Signals. *Materials*, *15*(7), 2659. https://doi.org/10.3390/ma15072659

[9] Topolář, L., Kocáb, D., Pazdera, L., & Vymazal, T. (2021). Analysis of Acoustic Emission Signals Recorded during Freeze-Thaw Cycling of Concrete. *Materials*, *14*(5), 1230. https://doi.org/10.3390/ma14051230

[10] Su, Y., Dong, L., & Pei, Z. (2022). Non-Destructive Testing for Cavity Damages in Automated Machines Based on Acoustic Emission Tomography. *Sensors*, *22*(6), 2201. https://doi.org/10.3390/s22062201

[11] Machikhin, A., Poroykov, A., Bardakov, V., Marchenkov, A., Zhgut, D., Sharikova, M., Barat, V., Meleshko, N., & Kren, A. (2022). Combined Acoustic Emission and Digital Image Correlation for Early Detection and Measurement of Fatigue Cracks in Rails and Train Parts under Dynamic Loading. *Sensors*, *22*(23), 9256. https://doi.org/10.3390/s22239256

[12] Gupta, M., Khan, M. A., Butola, R., & Singari, R. M. (2021). Advances in Applications of Non-Destructive Testing (NDT): A review. *Advances in Materials and Processing Technologies*, *8*(2), 2286–2307. https://doi.org/10.1080/2374068x.2021.1909332

[13] Wang, K., Liu, G., Li, Y., Qin, M., & Wang, G. (2019). Experimental evaluation of sand particle identification in oil–water–gas multiphase flows based on vibration signal analysis. *Chemical Engineering Research and Design*, *151*, 79–90. https://doi.org/10.1016/j.cherd.2019.07.029

[14] De Almeida, V., Serris, E., Cameirão, A., Herri, J.-M., Abadie, E., & Glénat, P. (2022). Monitoring gas hydrates under multiphase flow in a high pressure flow loop by means of an acoustic emission technology. *Journal of Natural Gas Science and Engineering*, *97*, 104338. https://doi.org/10.1016/j.jngse.2021.104338

[15] Siman-Tov, S., & Brodsky, E. E. (2021). Distinguishing between rheophysical regimes of fluid-saturated granular flows using dilatancy and acoustic emission measurements. *Granular Matter*, *23*(2). https://doi.org/10.1007/s10035-021-01103-8

[16] Lin, W., Wang, K., Yang, Y., Huang, Z., Sun, J., Wang, J., & Yang, Y. (2020). Characterization of flow pattern of cohesive particles in gas-solid fluidized bed via axial distribution of particle motions. *International Journal of Multiphase Flow*, *130*, 103355. https://doi.org/10.1016/j.ijmultiphaseflow.2020.103355

[17] Al-Lababidi, S., Mba, D., & Addali, A. (2012). Upstream multiphase flow assurance monitoring using acoustic emission. Acoustic Emission, 27, 217–250. https://doi.org/10.5772/31332

[18] W. Qin. (2022). Signal Analysis of Characteristics Using Passive Acoustic Emission Technique in Gas-Solid Pipeline Flows. Discrete Dynamics in Nature and Society, 2022, 7848008. https://doi.org/10.1155/2022/7848008

[19] Wang, K., Liu, G., Li, Y., Qin, M., Wang, J., Wang, G., & Mei, D. (2019). Vibration and acoustic signal characteristics of solid particles carried in sand-water two-phase flows. *Powder Technology*, *345*, 159–168. https://doi.org/10.1016/j.powtec.2018.12.092

[20] Kang, P., Lu, Y., Yang, L., Liu, L., Hu, X. (Eric), Luo, X., Chen, H., Zhou, Y., & Zhang, R. (2020). Nonlinear characteristics analyses of particle motion for predicting flow regimes. *Particuology*, *53*, 134–141. https://doi.org/10.1016/j.partic.2020.03.008

[21] Zhou, Y., Xu, Z., Xiao, G., Hu, X., Chen, H., Zhang, R., Luo, X., Wang, J., & Yang, Y. (2020). Monitoring the hydrodynamics and critical variation of separation efficiency of cyclone separator via acoustic emission technique with multiple analysis methods. *Powder Technology*, *373*, 174–183. https://doi.org/10.1016/j.powtec.2020.06.053

[22] Li, C., Zhu, Y., Wang, J., Liu, W., Fang, L., & Zhao, N. (2023). Mass flow rate measurement of gas-liquid two-phase flow using acoustic-optical-Venturi multisensors. *Flow Measurement and Instrumentation*, *90*, 102314. https://doi.org/10.1016/j.flowmeasinst.2023.102314

[23] Diao, X., Jiang, J., Shen, G., Chi, Z., Wang, Z., Ni, L., Mebarki, A., Bian, H., & Hao, Y. (2020). An improved variational mode decomposition method based on particle swarm optimization for leak detection of liquid pipelines. *Mechanical Systems and Signal Processing*, *143*, 106787. https://doi.org/10.1016/j.ymssp.2020.106787

[24] Liu, T., Jin, Y., Wang, S., Zheng, Q., & Yang, G. (2023). Denoising method of weak fault acoustic emission signal under strong background noise of engine based on autoencoder and wavelet packet decomposition. *Structural Health Monitoring*, *22*(5), 3206–3224. https://doi.org/10.1177/14759217221143547

[25] Yu, A., Liu, X., Fu, F., Chen, X., & Zhang, Y. (2023). Acoustic Emission Signal Denoising of Bridge Structures Using SOM Neural Network Machine Learning. *Journal of Performance of Constructed Facilities*, *37*(1). https://doi.org/10.1061/(asce)cf.1943-5509.0001778

[26] Kim, J., Harne, R. L., & Wang, K. W. (2022). Online Signal Denoising Using Adaptive Stochastic Resonance in Parallel Array and Its Application to Acoustic Emission Signals. *Journal of Vibration and Acoustics*, *144*(3). https://doi.org/10.1115/1.4052639

[27] Huang, Y., Wang, K. H., & Zhou, X. X. (2018). Translation Invariant Wavelet De-noising of CO_2 Gas Shielded Arc Welding Electrical Signal. *Journal of Mechanical Engineering*, *54*(8), 95–100. https://doi.org/10.3901/JME.2018.08.095

[28] de Oliveira, E. M., & Cyrino Oliveira, F. L. (2018). Forecasting mid-long term electric energy consumption through bagging ARIMA and exponential smoothing methods. *Energy*, *144*, 776–788. https://doi.org/10.1016/j.energy.2017.12.049

[29] Kim, J., & Jung, H. (2017). Time series forecasting using functional partial least square regression with stochastic volatility, GARCH, and exponential smoothing. *Journal of Forecasting*, *37*(3), 269–280. https://doi.org/10.1002/for.2498

[30] Jia, R.-S., Liu, C., Sun, H.-M., & Yan, X.-H. (2015). A situation assessment method for rock burst based on multi-agent information fusion. *Computers & Electrical Engineering*, *45*, 22–32. https://doi.org/10.1016/j.compeleceng.2015.04.015

[31] Akhoundi, M. A. A., & Valavi, E. (2019). Multi-Sensor Fuzzy Data Fusion Using Sensors with Different Characteristics. *The CSI Journal on Computer Science and Engineering*. *16*(2), 44-53. https://doi.org/10.48550/ARXIV.1010.6096

[32] Fu, H. Q., Zhu, J. J., Wang, C. C., Wang, H. Q., & Zhao, R. (2018). A Wavelet Decomposition and Polynomial Fitting-Based Method for the Estimation of Time-Varying Residual Motion Error in Airborne Interferometric SAR. *IEEE Transactions on Geoscience and Remote Sensing*, *56*(1), 49–59. https://doi.org/10.1109/tgrs.2017.2727076

[33] Phillips, R. C., & Gorse, D. (2018). Cryptocurrency price drivers: Wavelet coherence analysis revisited. *PLOS ONE*, *13*(4), e0195200. https://doi.org/10.1371/journal.pone.0195200

[34] Chen, S., Meng, H., Zhong, Q., & Li, X.-Y. (2018). Microseismic data SNR enhancement using local projection denoising method. *Journal of Geophysics and Engineering*, *15*(6), 2566–2576. https://doi.org/10.1088/1742-2140/aadb73

[35] Zhu, J., Zhang, Z., & Kuang, C. (2015). A Reliable Evaluation Indicator of Wavelet Denoising. Journal of Wuhan University (Geomatics and Information Science), *40*(5), 688-694. https://doi.org/10.13203/j.whugis20130417

[36] Jian, S., & Wen, W. (2017, February). Study on underwater image denoising algorithm based on wavelet transform. In *Journal of Physics: Conference Series* (Vol. 806, No. 1, p. 012006). IOP Publishing. https://doi.org/10.1088/1742-6596/806/1/012006.

[37] Li, L., & Si, Y. (2018). Enhancement of Medical Images Based on Guided Filter in Nonsubsampled Shearlet Transform Domain. *Journal of Medical Imaging and Health Informatics*, *8*(6), 1207–1216. https://doi.org/10.1166/jmihi.2018.2469

[38] Li, Z. C., Deng Y., Zhang, G. Y., & Yang, X. H. (2011). Determination of best grading of wavelet transform in deformation measurement data filtering. *Geomatics and Information Science of Wuhan University*, *36*(3), 285–288. https://doi.org/10.13203/j.whugis2011.03.006

[39] Qu, G. Q., Dang, Y. M., & Zhang, C. Y. (2007). Uncertainty of de-noising of deformation monitoring signals. *Science of Surveying and Mapping*, 32, 21–22.

Lide Fang received a B.Sc. degree from China Jiliang University, Hangzhou, China, in 1998, an M.Sc. degree from Hebei University of Technology, Tianjin, China, in 2005, and a Ph.D. degree from Tianjin University, Tianjin, China, in 2008. Since 1998, he has been with the Quality and Technical Supervision College, Hebei University, Baoding, China. He is currently a Professor and a Ph.D. supervisor. He has authored or co-authored over 100 articles in core journals and above, receiving 80 patents. His current research interests include multiphase flow measurement technology and instruments.

Yue Feng received a B.Sc. degree from Hebei University, Baoding, China, in 2014, and an M.Sc. degree from Tianjin University, Tianjin, China, in 2017. She is currently pursuing her Ph.D. degree at Hebei University, Baoding, China. She is currently a Lecturer at Langfang Normal University, Langfang, China. Her research interests include multiphase flow simulation, liquid-solid two-phase flow parameters measurement, and flow mechanism analysis.

Jianzhang Sun the B.Sc. degree from Industrial and Commercial College, Hebei University, Hebei, China, in 2019, and the M.Sc. degree from Hebei University, Baoding, China, in 2024. His main research interest is multiphase flow measurement technology and instruments during the graduate study, now his main works in metrology, including acoustics, electromagnetism.

Qiaoqiao Zeng received a B.Sc. degree from Cangzhou Normal University, Cangzhou, China, in 2017, and a M.Sc. degree from Hebei University, Baoding, China, in 2020. She is currently a metrological engineer at Hubei Huangshi Institute of Measurement and Testing, Huangshi, China. Her main research interest is multiphase flow measurement technology and instruments during her graduate study, now her scientific work focuses on metrology, including acoustics, mechanics and the like.

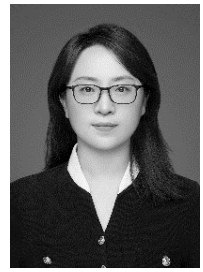

Fang Dong received a B.Sc. degree from Hebei University of Science and Technology, Shijiazhuang, China, in 2003, and an M.Sc. degree from Tianjin University, Tianjin, China, in 2007. Since 2007, she has been with the Quality and Technical Supervision College, Hebei University, Baoding, China. Her main research interests include multiphase flow theory and flow parameter detection technology.

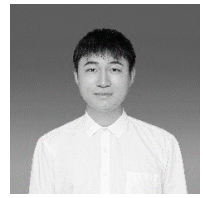

Meng Zheng received the B.S. degree from Hebei University, Baoding, China, in 2020, where he is currently pursuing the M.S. degree. His current research interest includes multiphase flow measurement technology and instruments.